Invited paper

Intra- and inter-cell interference investigations for broadband radio access systems above 10 GHz

Ranjan Bose, Andreas Hayn, and Rolf Jakoby

Abstract — Local multipoint distribution systems (LMDS) operating above 10 GHz have a large bandwidth (2–3 GHz) but a very limited range. These systems can provide coverage to a few kilometers only. The size of the macro cells illuminated by the base stations, where line of sight (LOS) exists, is 1 to 6 km. To provide coverage to customers where LOS is not possible, repeaters or passive reflectors may be used. In this paper we present first results of reflection measurements at 42 GHz, and based on that, simple multipath studies, taking into account the beamwidth of the antennas of both, transmitter and receiver. Secondly, LOS cochannel and adjacent channel interference are assessed for cellular LMDS networks. As suggested in the CRABS report, the maximal spectral efficiency can be obtained with a dual frequency and polarization reuse plan. This frequency and polarization reuse leads to interference. In this paper we have first calculated the cochannel interference (CCI) and the adjacent channel interference (ACI) due to the frequency/polarization reuse schemes suggested in the CRABS report. The effects of the variation of the half power beam width (HPBW) of the receiver, the time percentage parameter *p*, and the cell radius on *C/I* are also reported. In the latter part of the paper we propose a simple interference reduction technique based on re-orientation of the receiver antennas. We have also explored the possibility of using trellis coded modulation (TCM) for reducing interference levels. Initial results have been found to be quite encouraging.

Keywords — multipath propagation, interchannel interference.

1. Introduction

Broadband radio access systems operating at millimeter waves, used for local multipoint distribution service, have a large bandwidth of up to 2 GHz but a very limited coverage to a few kilometers only [1 ÷ 3]. This is mainly because they require clear line of sight between the base station and the subscriber antennas as well as because millimeter waves suffer on large propagation losses, particularly free-space propagation losses and attenuation caused by rain. However, in urban areas, the LOS requirements and the capacity needed for interactive services are more likely to limit the maximum cell size than the basic radio propagation characteristics [2, 3]. To enhance coverage to customers where LOS is not possible, passive and active repeaters may be used [4].

To compete successfully with the standard broadcasting, cable and satellites, the signals in the LMDS architecture need to be reliable and of high quality. The critical propagation issues are clear air absorption, signal attenuation by rain, vegetation and buildings, signal depolarization, multipath and cell-to-cell interference [5]. In Section 2 of this paper we investigate reflection and multipath effects and in Section 3 LOS cochannel and adjacent channel interference problems for broadband radio access systems above 10 GHz. The last section starts with the description of the LMDS system under study. Its first Subsection 3.1 deals with the LOS interference calculations. The effects of varying the receiver antenna beamwidth, the cell radius and the time percentage are reported in this section. In Subsection 3.2 we propose a simple technique for the reduction of cochannel interference by reorientation of the receiver antenna. Reorientation under the constraint of system availability is discussed in Subsection 3.3. The paper concludes by a discussion of the results in Section 4.

2. Reflection and multipath effects

Within LMDS cells we usually have a low penetration rate especially in urban areas. This is caused by the obstruction due to buildings, vegetation etc. An inexpensive option to increase penetration might be the usage of reflected waves into non-line-of-sight (NLOS) areas, if the reflection losses are smaller than a certain available system margin. This might be an option, especially in the vicinity of the hub below a radius of about 2 km where the system margin can be larger than 20 dB [6]. Besides the usage of such reflected waves, they always generate additional interference due to multipath propagation. For both, it is of interest to model the reflection losses realistically.

2.1. Reflection measurements

The reflecting wall or ground can be simply modeled in a first step by the Fresnel reflection coefficients for a plain dielectric surface and for perpendicular and parallel polarization:

$$R_{\parallel} = \frac{\sqrt{\underline{\varepsilon}_2 - \sin^2(\vartheta_{in})} - \underline{\varepsilon}_2 \cdot \cos(\vartheta_{in})}{\sqrt{\underline{\varepsilon}_2 - \sin^2(\vartheta_{in})} + \underline{\varepsilon}_2 \cdot \cos(\vartheta_{in})};$$

$$R_{\perp} = \frac{\cos(\vartheta_{in}) - \sqrt{\underline{\varepsilon}_2 - \sin^2(\vartheta_{in})}}{\cos(\vartheta_{in}) + \sqrt{\underline{\varepsilon}_2 - \sin^2(\vartheta_{in})}}, \qquad (1)$$

with the complex permittivity $\underline{\varepsilon}_2 = \varepsilon_2\,(1 - j\,\tan\,(\delta))$ of the dielectric material and the angle of incidence ϑ_{in} (Fig. 1). In a second step we assumed a slightly rough surface with Gaussian distributed roughness [8], having a standard deviation $\sigma_h < \lambda$. This leads to the following reduction coefficient [9]:

$$\rho(x) = e^{-x} \cdot I_0(x), \quad x = 8 \cdot \left(\frac{\pi \sigma_h \cos(\vartheta_{in})}{\lambda} \right)^2, \quad (2)$$

where I_0 is the modified Bessel function of the order zero and hence to the following modified Fresnel reflection coefficients:

$$R_{\|\text{rough}} = R_{\|} \cdot \rho\,; \quad R_{\perp\text{rough}} = R_{\perp} \cdot \rho\,, \quad (3)$$

which exhibits very good agreement with measurements of slightly rough and large surfaces compared to λ.

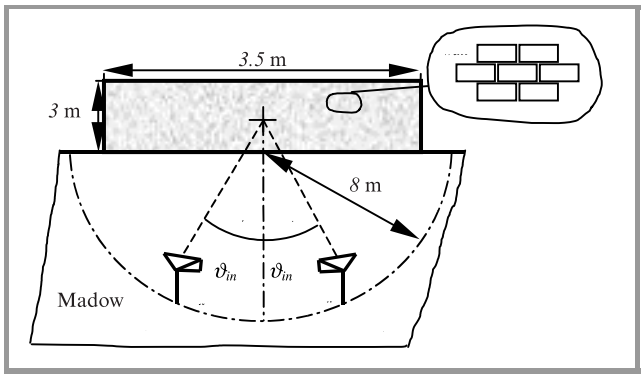

Fig. 1. Systematic reflection measurements on a brick wall.

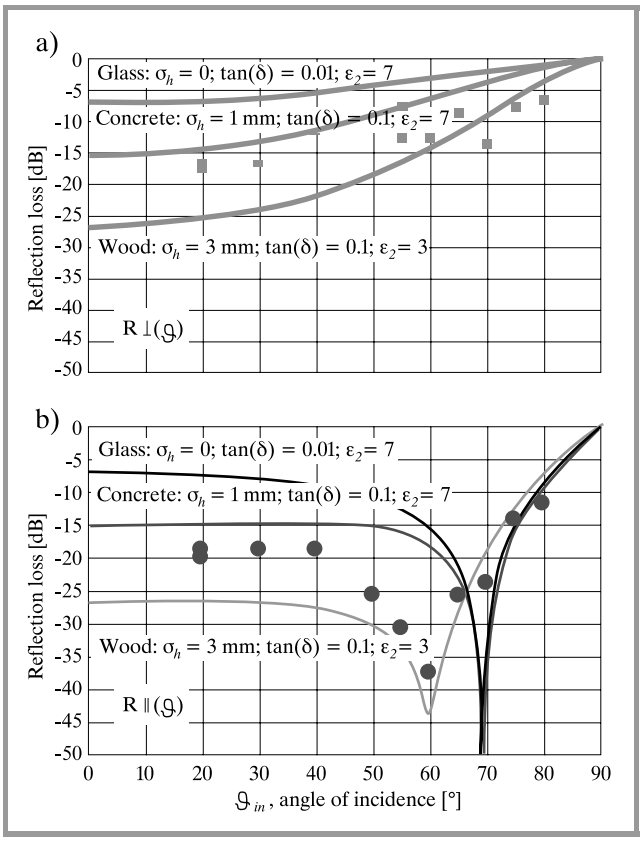

Fig. 2. Measured reflection loss of a brick wall and the modified Fresnel reflection losses for glass, concrete and wood for perpendicular polarization $R_{\perp}(\vartheta)$ (a) and parallel polarization $R_{\|}(\vartheta)$ (b) at 42 GHz.

For 42 GHz, Fig. 2 shows some results of systematic 2D-measurements of the bistatic reflection profile for $R_{\perp}(\vartheta)$ and $R_{\|}(\vartheta)$ from a brick wall with an average value of $\sigma_h \approx \lambda/7$, which was carried out by a measurement setup schematically shown in Fig. 1. Since the electric properties of the brick wall were not exactly known, we compared these measurements with the reflection losses calculated with Eq. (3) for three different materials: glass, concrete and wood. The measured reflection losses exhibits similar behavior vs. the angle of incidence as the calculated modified Fresnel reflection losses and are mostly in between the curves for concrete and wood, indicating of course, a large spread of about 5 dB due to some measurement uncertainties like slight misalignment of the very directional receiving antenna, temperature effects of the measurement equipment etc.

In order to model the reflection losses more realistically for LMDS scenarios, several systematic 3D-reflection measurements at 42 GHz were carried out at buildings in real environments with different materials, structures and surface roughness σ_h in dependence of the angle of incidence and along several measurement paths. One scenario is shown in Fig. 3a, where the LMDS transmitter was located at the top of a high building at 46.2 m and the received power of the reflections from a building front was recorded along the measurement path l at a height of 1.8 m above ground. The received power due to reflections from the building front along the path is indicated by the bars in Fig 3b. The variation in the received power of up to about 5 dB was partly caused by time variant effects like moving transmitter, receiver and vegetation being within the path due to wind forces as well as small alterations in the alignment of the receiving antenna around the direction where the maximum level was found.

To analyze 3D-reflections and to compare these measurements with prediction, two theoretical curves have always been plotted in addition: the free-space attenuation due to the wave travelling from the transmitter via the reflection point to the receiver (curve at the top) and this free-space attenuation plus the reflection loss (curve at the bottom). This last factor was calculated by firstly splitting up the incident field strength vector into parallel and perpendicular components to the plane of incidence, and then weighting both components with the corresponding modified Fresnel reflection coefficients for concrete according to Eq. (3). After that, the total field strength is given by summing up both vectors and hence the received power can be predicted by taking into account the polarization mismatch with the

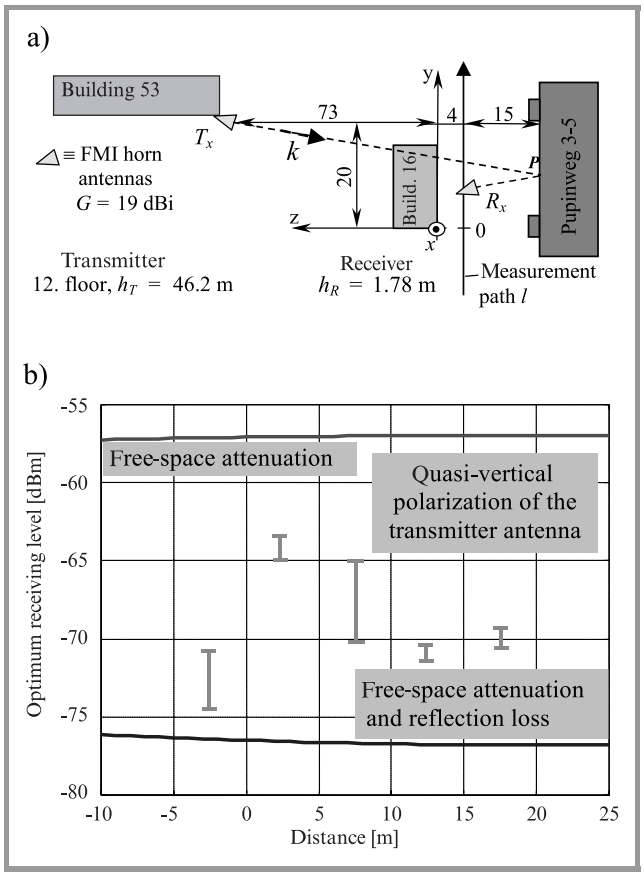

Fig. 3. (a) Typical LMDS scenario for measuring reflections from buildings; (b) received power of reflected waves recorded along a measurement path l in comparison with two theoretical curves.

receiving antenna, as well as the additional free-space attenuation. As we can see from Fig. 3b, all measured power levels (bars) are several dB above this predicted curve at the bottom, which has been valid for nearly all measurements. One reason for this higher measured levels than predicted for concrete ($\sigma_h = 1$ mm, $\tan(\delta) = 0.01$, $\varepsilon_2 = 7$) is of course, that all buildings consist of a mixture of different materials, in particular of concrete and glass, but also wood and metal frames. A second reason is that an exact alignment of the receiver antenna on the theoretical reflecting point of the buildings was very difficult. Therefore, we simply looked for the maximum of the received reflected power even it was found apart from the theoretical reflection line. This maximum is often caused by areas of the buildings with smooth window panes and metallic window frames, having relatively low reflection losses, and thus increasing the measured power levels compared to the predicted ones by assuming purely concrete with rough surfaces. Hence, these predicted curves for concrete walls are usually to pessimistic.

Beside that, our 2D- and 3D-measurements indicate, that on principle, the relatively strong reflections (except in the region of the Brewster angle for the parallel polarization) could be used to enhance the area coverage also into the NLOS areas when the system margin is sufficient. Thus, increasing the penetration rate of LMDS cells. Unfortunately, good reflectors of buildings are often windows, which are not reliable, because they can be opened and hence changing its scattering features. Hence, for using natural reflections, it has to be ensured that they are caused dominantly by static walls. A reliable option to enhance penetration into shadowed regions is the use of elliptical reflectors as passive repeaters [10].

2.2. Multipath propagation

Apart from using natural reflections to enhance penetration, strong reflections have always to be considered in conjunction with multipath propagation. This is generally agreed to be neglectable for LMDS, because of the very directional antennas of the customers, having half power beam widths usually in between 2° and 5°. But even, if the probability might be low to catch some multipath propagation components within this *HPBW*, there will partly be interference, if just one reflected wave in addition to the direct wave will be received within the *HPBW* of the customer antennas. Thus, it should be considered for the design of the equalizer of the receiver. Based on the reflection measurements and modeling those reflections for rough surfaces above, we carried out a worst-case estimation with a simple two-ray model according to the geometric arrangement in Fig. 4, assuming only one "optimally"-oriented slightly rough dielectric surface (dielectric reflector), which might be a building wall or a roof.

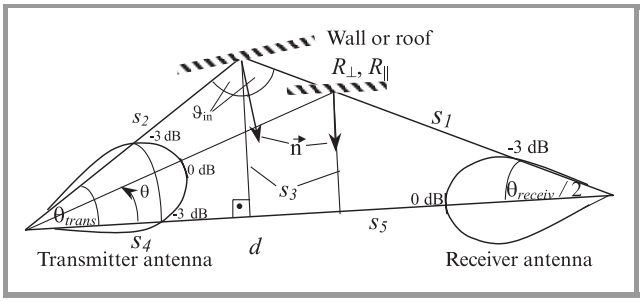

Fig. 4. Simple geometry for the estimation of worst-case multipath propagation (two-ray model).

For this simple arrangement, the direct ray is defined to go through the -3 dB point of the transmitter antenna and hits the maximum of the receiver antenna, whereas the reflected ray goes through an arbitrary point within the *HPBW* of the transmitter antenna under the angle θ, hits law of reflection and then cuts the receiver antenna at the -3 dB decay point. Hence, the antennas are sufficiently described by their *HPBW* θ_{trans} and θ_{receiv} and the antenna pattern of the transmitter within its *HPBW*, which is approximated by $\sin^2(\pi/4 + \theta)$ with $\theta \in [0, \pi/2]$ for the 90°-antenna. By the use of this simple geometrical arrangement, the magnitudes of both rays at the receiver, the relative time delay between the direct and the reflected waves as well as

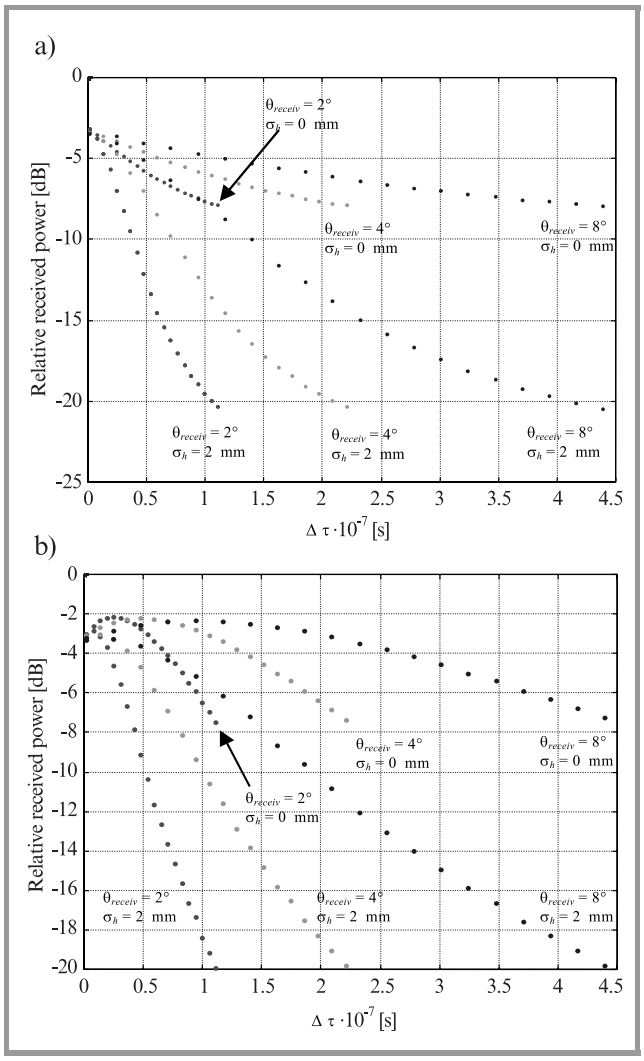

Fig. 5. Power delay profiles at the receiver with respect to the relative attenuation of the reflected path compared to the direct wave in dB with various roughness σ_h of the wall and *HPBW* Θ_{receiv} of the receiver antenna: (a) without considering a specific antenna pattern of the transmitter; (b) taking into account the $\sin^2(\pi/4+\theta)$ antenna pattern of the transmitter.

the power delay profiles were estimated for certain materials of the dielectric reflector in dependence of the distance d between the transmitter and receiver and the *HPBW*'s of both, the transmitter and receiver antennas. The relative time delay is:

$$\Delta\tau = \left(\frac{s_3}{\sin(\theta_{receiv}/2)} + \frac{s_3}{\sin(\theta)} - d\right)\cdot c^{-1},$$
$$\text{with} \quad s_3 = \left[\frac{1}{\tan(\theta_{receiv}/2)} + \frac{1}{\tan(\theta)}\right]\cdot d^{-1}. \qquad (4)$$

For typical LMDS receiver antennas with $\theta_{receiv} < 8°$, use can be made by the following linear approximation:

$$\Delta\tau \approx 0.32\cdot 10^{-3}\cdot\theta\cdot\theta_{receiv}\cdot d \quad [\text{ns}], \qquad (5)$$

where the parameters θ_{receiv} and θ are given in degrees and d in meter. The estimation error for this approximation remains low up to about $\theta_{receiv} = 16°$, where it exceeds 13%. For example, assuming $\theta_{trans} = 90°$, $\theta_{receiv} = 4°$ and a distance d of 2 km, the maximum relative delay $\Delta\tau_{max}$ can be 230 ns (i.e. if $\theta = \theta_{trans}$). So, even for narrow customer antenna pattern, this delay can be several times of the symbol rate of a QPSK-signal within a LMDS specific bandwidth of 33 MHz, which cannot be ignored for system design. It can easily be seen from Fig. 4 and Eq. (5), that each delay value $\Delta\tau$ has its corresponding value of the angle θ and hence, angle of incident on the reflecting surface:

$$\vartheta_{in} = \frac{1}{2}(180° - \theta_{receiv}/2 - \theta)\,. \qquad (6)$$

With this angle of incidence ϑ_{in}, the reflection losses can be estimated by the use of Eq. (3). As a worst-case estimation of a power delay profile, this has only been carried out for the perpendicular polarization, having less losses than the parallel polarization according to Fig. 2.

The envelope of the power delay profile can easily be derived with the close relationship between $\Delta\tau$ and this modified Fresnel reflection coefficient $R_\perp(\vartheta)$ due to the fixed geometrical arrangement according to Fig. 4. In a first iteration, it has not been taken into account a specific antenna characteristic of the transmitter antenna within $\theta_{trans} = 90°$. For the antenna configuration shown in Fig. 4, Fig. 5 shows the total received power at 42 GHz with respect to the one of the direct wave in dependence of the relative path delay $\Delta\tau$ for different θ_{receiv} and σ_h (e.g. glass and concrete), but fixed distance d = 2 km. It can be seen from Fig. 5a, that the envelope of the relative losses (i.e. power delay profile) is nearly proportional to the relative delay $\Delta\tau$ and θ_{receiv} of the receiver antenna. Taking into account the specified 90°-transmitter antenna characteristics and the other parameters as mentioned before, the power delay profiles in Fig. 5b are even worse. Comparing our results, the two ray models proposed in the IEEE 802.16 [11] standard are potentially to optimistic.

3. LOS interference

In this paper, we present the LOS calculations for the cell areas affected by the cochannel interference and the adjacent channel interference for a cellular LMDS architecture suggested by Telenor in the CRABS report [1, p. 46], which yields the same results as for a similar scheme proposed by Deutsche Telekom in [2]. In both, the maximal spectral efficiency was obtained with a dual frequency and polarization reuse plan according to Fig. 6, where the macrocells are square in shape. For this architecture, the cochannel cells appear in the 5th tier. The 42-GHz-LOS-interference calculations are done based on a H-plane or E-plane sectoral horn antennas for the transmitter at the base stations, providing horizontal and vertical polarization, respectively. The transmitter antennas have a half power beam width approximately equal to 90°. The receiver antennas of the subscribers are assumed to have a circular aperture with a parabolic taper on pedestal with a 10 dB

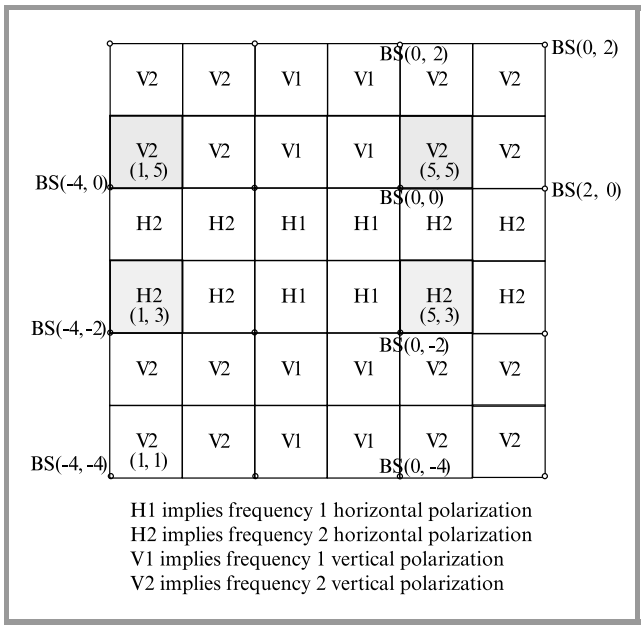

Fig. 6. Dual frequency and polarization reuse plan as suggested in the Telenor scheme of the CRABS report [1]. The circles in the figure denote the position of the base stations, on which four 90°-sectoral horn antennas are mounted. The two closest cells experiencing CCI are labeled (5, 5) and (1, 5) and those cells experiencing ACI are labeled (5, 3) and (1, 3), assuming the interfering cell is (1, 1).

edge illumination, having high gain between 30 to 40 dB with a very narrow *HPBW* of 5° to 2° for a diameter of about 10 to 24 cm.

The cochannel interference has been calculated for LOS under clear weather conditions without any power control strategy (worst case) using the formula:

$$C/I(L, L_2, p) = [EIRP - EIRP_1] + [G_R(0) - G_R(\theta)] + \\ -[L_{fs}(L) - L_{fs}(L_2)] - [A_{cs}(L) - A_{cs}(L_2)] + \\ -A_f(L_2, p) \quad [\text{dB}], \tag{7}$$

where $EIRP$ and $EIRP_I$ are the equivalent isotropic radiated powers of the desired and interfered signals at the customer location, $G_R(\theta)$ is the receiver antenna gain at an angle θ off the boresight, L_{fs} is the free space path loss, A_{cs} is the attenuation during clear sky, A_f is the short term enhancement due to atmospheric multipath and focussing effects, p is the time percentage for which A_f exceeds a certain value [2], L and L_2 are the distances in km from the base station of the desired and cochannel cell, respectively. At 42 GHz, A_{cs} has been taken as 0.2 dB/km [4, p. 92]. The short term enhancement due to atmospheric multipath and focussing effects, A_f, is determined using the formula [2]:

$$A_f = 2.6(1 - e^{-L/10}) \log_{10}(p/50). \tag{8}$$

3.1. LOS interference calculations

Numerical simulation was carried out to determine the percentage of areas where the C/I was above a specified threshold. Simulations were carried our both for cochannel and adjacent channel interference. The C/I levels of interest were 10, 15, 20, 25 and 3 dB, depending on the operating modulation scheme (QPSK, 8-PSK, 16-QAM or even 64-QAM).

The percentage of cell area below these C/I threshold levels are given in Table 1. The simulation takes into account a squared cell dimension $L = 2$ km, a time percentage $p = 0.01\%$ for which short term enhancement due to atmospheric multipath and focussing effects, A_f, exceeds 6.51 dB according to Eq. (8), and a receiving antenna of the customer with a diameter of 10 cm, i.e. an antenna gain of about 30 dB and a $HPBW$ of about 5°. The areas within the cell that experience these C/I levels (as a percentage of the total cell area) are shown in Fig. 7. Figure 7a gives the regions experiencing high CCI values while Fig. 7b depicts the regions with high ACI.

Table 1
Approximate areas within the cell that experience different levels of CCI

C/I value in cell (5, 5) [dB]	Approximate areas [%]	
	CCI	ACI
Below 10	5.48	0.14
Below 15	15.14	1.45
Below 20	22.24	4.80
Below 25	27.33	13.80
Below 30	29.87	24.85
Above 30	70.12	75.15

Next, simulations were carried out for different receiver antenna diameters/*HPBW* to see the effect of increasing the receiver antenna beamwidth. The results are given in Table 2. For these simulations, the transmitter is a H-plane sectoral horn and the receiver is a dish with a parabolic squared aperture. Interference from the most dominant cochannel cell has been considered only. The transmitter antenna characteristics are: $HPBW = 88°$, $A = 0.46$ cm ($0.65\ \lambda$), $R_1 = 2.00$ cm. For the simulation, the time percentage, $p = 0.01$ and the cell radius = 2 km.

In order to observe the effect of the time percentage, p, on the C/I, the parameter p was varied from 0.001% to 10%. The results are given in Table 3. It can be seen from the table that p, which has an effect on A_f (the short term enhancement due to multipath and focussing effects), has an important role to play in the determination of C/I. When we relax the time percentage parameter to even 0.1%, the C/I does not fall below 10 dB. However, p has a less severe effect on higher C/I. For example, a change in p from 0.001% to 10% causes the area where $C/I < 15$ dB to change by 89%, the area where $C/I < 20$ dB to change by 48% and the area where $C/I < 30$ dB to change by only 7%. Thus, the effect of p should not be neglected for low C/I.

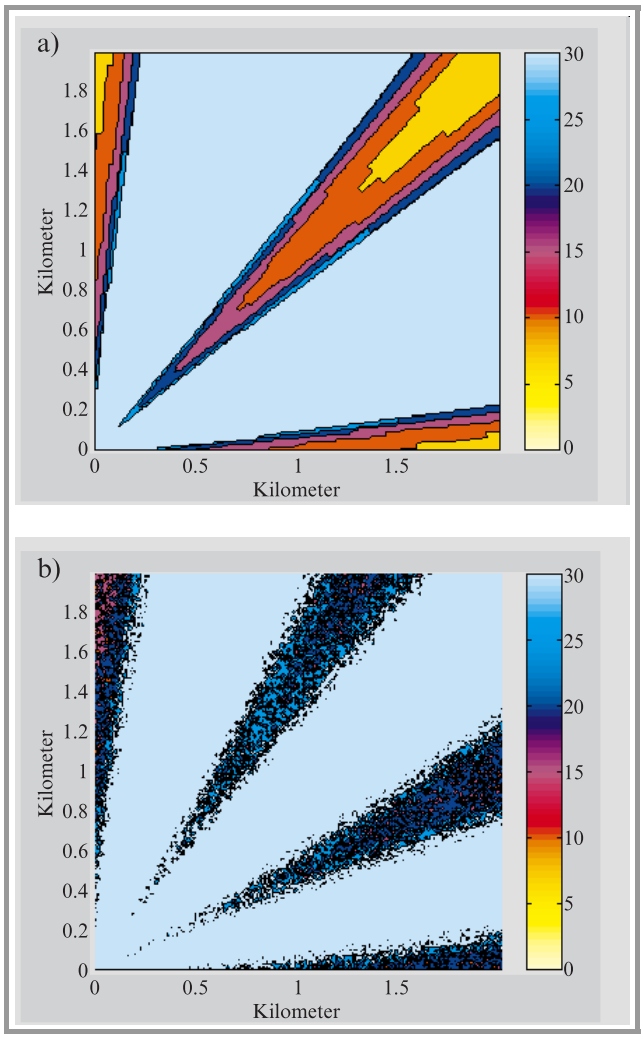

Fig. 7. Color coded areas within the cell (5, 5) that experience C/I levels below a specified level for (a) CCI and (b) ACI. The units of the color bar is in dB. The squared cell dimension is $L = 2$ km, the time percentage $p = 0.001\%$ for which A_f exceeds 7.81 dB and the *HPBW* of the receiver antenna is 5°.

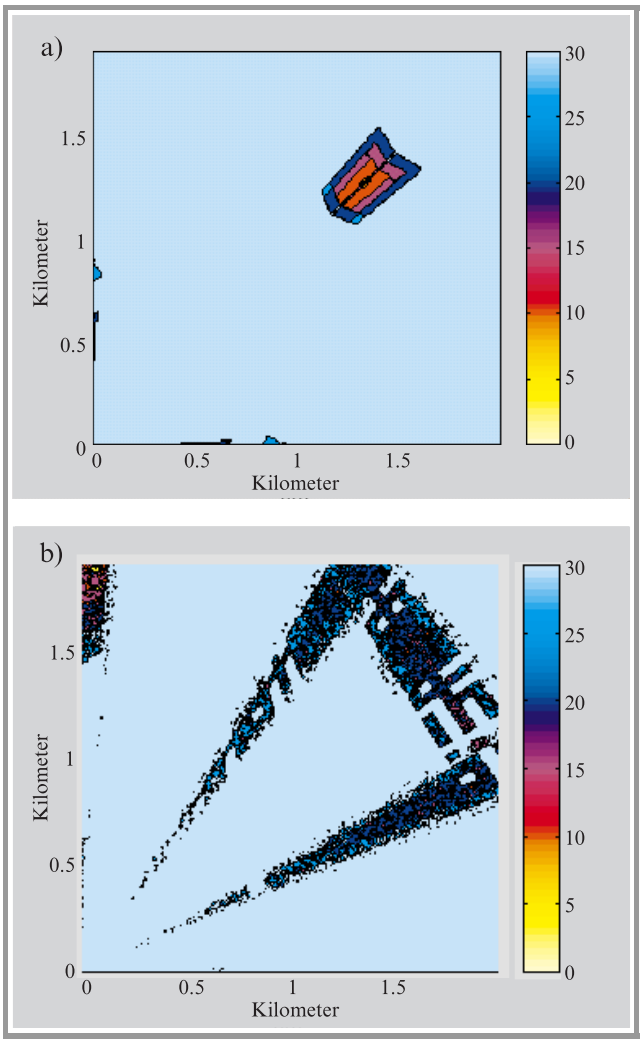

Fig. 9. The areas experiencing high levels of CCI (a) and ACI (b) in cell (5, 5) in the Telenor scheme after reorientation of receiver antennas. The units of the color bar is in dB. The *HPBW* of the $T_x = 88°$, that of the $R_x = 3°$, $p = 0.001$, cell radius = 2 km.

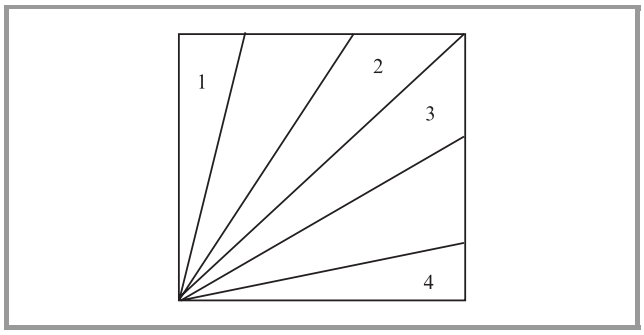

Fig. 8. The four disjoint wedges in which the receivers are reoriented.

Next, the effect of varying the cell radius on the interference was analyzed. The cell radius also plays a crucial role in the calculation of C/I. It has been mentioned earlier, the cell radius in the LMDS architecture can range from 1 to 10 km. Simulations were performed to find out the variation of C/I with the cell radius. The radius of the cell was varied from 0.5 to 15 km and the results are given in Table 4.

It can be observed from the table that the areas where the C/I is below a specified level at first increases with the increase in the cell radius. It reaches a maximum and then starts to decrease. The cell radius that results in the minimum C/I (i.e., the maximum areas experiencing high interference) is approximately 3 km, for the simulation parameters considered here. This behavior can be explained as follows. At very low values of the cell radius, the free space path loss, A_{fs}, is the dominant factor. As the cell radius increases, the short term enhancement due to multipath and focussing effects, A_f, starts playing a dominant role and increases the interference level. As we increase the cell radius further, the increase in the interference due to A_f is compensated by the free space path loss, A_{fs}. Consequently, the total interference starts decreasing.

Table 2
Percentage of areas below a specified C/I ratio in cell (5, 5)

R_x antenna		Cell (5, 5)				
Diameter [cm]	*HPBW* [°]	$C/I < 10$ dB	$C/I < 15$ dB	$C/I < 20$ dB	$C/I < 25$ dB	$C/I < 30$ dB
24	2.0	0.15	1.08	1.52	1.95	2.51
20	2.4 (CRABS)	0.82	4.44	7.22	8.93	9.40
10	4.7	1.94	8.52	13.08	15.59	18.41
9.6	5.0	2.00	8.99	13.85	16.97	19.05

Table 3
Percentage of areas below a specified C/I ratio in cell (5, 5) (diameter of the receiver = 20 cm, $HPBW = 2.4°$)

Time percent, p [%]	$C/I < 10$ dB	$C/I < 15$ dB	$C/I < 20$ dB	$C/I < 25$ dB	$C/I < 30$ dB
0.001	2.68	4.99	8.12	9.17	9.47
0.01	0.61	4.23	6.85	8.83	9.38
0.1	0	3.55	5.65	8.53	9.29
1.0	0	1.92	4.84	7.86	9.12
10	0	0.51	4.20	6.71	8.84

Table 4
Percentage of areas below a specified C/I ratio in cell (5, 5) (diameter = 20 cm, $HPBW = 2.4°$, $p = 0.01\%$)

Cell radius [km]	$C/I < 10$ dB	$C/I < 15$ dB	$C/I < 20$ dB	$C/I < 25$ dB	$C/I < 30$ dB
0.5	0	2.00	4.88	7.92	8.88
1.0	0	3.54	5.49	8.48	9.25
2.0	0.61	4.23	6.85	8.83	9.38
3.0	0.71	4.36	7.06	8.89	9.40
5.0	0.28	3.95	6.29	8.74	9.36
10.0	0	0.51	4.22	6.75	8.87
15.0	0	0	0.59	4.32	6.92

3.2. Reducing CCI using reorientation of receiver antennas

Having investigated the LOS cochannel and adjacent channel interference problem, we now propose a simple technique for the reduction of areas within the cell experiencing high levels of interference. Let us assume that the current BS location is (0, 0) as given in Fig. 1. It should be noted that the coordinate system for the BS is different from that used for representing the cells. We need two different coordinate systems because the BS are not placed at the center of the cell, but at one of the corners. Hence, in many cases the same BS location is valid for four cells. From Fig. 7 we note that the regions of high interference roughly form wedges within the cell. There are three disjoint wedges where the interference levels are unacceptable due to the three cochannel cells: (1, 5), (1, 1) and (5, 1). The receivers in these regions of high interference can be reoriented to the BS of nearby cells in order to reduce interference levels. Here we have taken the cut-off $C/I = 30$ dB to label an area as a high interference zone. By simply observing the cells around the wedges that depict high interference regions, we choose the reorientation scheme as following. The receivers located in wedge 1 are reoriented to BS at (2, 2), those in the top section of wedge 2 to BS at (0, 2),

Table 5
After reorientation, the current and the interfering BS for the four wedges

Wedge	Current BS (after reorientation)	Interfering BS (CCI)		
		dominant	less dominant	
1	(2, 2)	(6, 6)	(10, 6)	–
2	(0, 2)	(−4, 10)	(−4, 6)	(−4, 2)
3	(2, 0)	(10, −4)	(6, −4)	(2, −4)
4	(2, 2)	(6, 6)	(6, 10)	–

those at the bottom half of wedge 2 to BS at (2, 0) and those in wedge 4 to BS at (2, 2). Thus, there are now four wedges from the point of view of reorientation, as depicted in Fig. 8. Due to reorientation, new cochannel cells come into picture. Table 5 gives the list of the new cochannel cells for the four wedges after reorientation.

As a first level interference estimation, only the dominant cochannel cell was considered for line of sight CCI calculations after reorientation. The areas facing high interference after reorientation is shown in Fig. 9. Table 6 compares the percentage of areas suffering from high CCI values before and after the reorientation scheme. If, upon reorientation of a receiver antenna the CCI worsens, it is reverted back to the original base station.

Since we make the best choice for a receiver regarding which BS it should point to, the reorientation strategy can only provide improvement. It can be seen in Fig. 9 that there are still some areas where, even after reorientation, the interference level is unacceptable. However, the levels are better than before. For example, the worst C/I value prior to reorientation was 6.65 dB, and after reorientation, the worst value is $C/I = 9.74$ dB (over 3 dB improvement, though still unacceptable).

We next look at the effect of reorientation of receiver antennas on adjacent channel interference. The process of reorientation to reduce CCI also results in new ACI cells. Table 7 lists the new cells that offer ACI as a result of reorientation in order to reduce the problem of CCI. The values of the resulting ACI due to the reorientation of R_x antennas is given in Table 8. The plot of the areas experiencing ACI is also shown in Fig. 9. From Table 3 it is clear that the process of reorientation has not reduced the ACI much. The values are comparable to those obtained prior to reorientation. This was expected as the strategy for reorientation of R_x antennas was to reduce CCI, and not ACI. It could be possible that there is a slight increase in the ACI values after reorientation.

Table 6
Approximate areas within the cell that experience different levels of CCI before and after reorientation of R_x antennas

C/I value [dB]	Approximate areas [%]	
	before reorientation	after reorientation
Below 10	3.52	0.04
Below 15	9.71	0.70
Below 20	13.05	1.56
Below 25	17.05	3.12
Below 30	19.12	3.47
Above 30	80.87	96.52

A more appropriate solution would be to check every R_x location and see whether the reorientation to reduce CCI or ACI produces a better result. The reorientation should be done accordingly. In many cases, one of the two, CCI or ACI increases and the other one decreases due to reorientation. Plus a third choice is not to go for reorientation. So the strategy should be to choose the best of the three possible solutions using the following decision rule: "Choose orientation to maximize the minimum of (CCI_i, ACI_i) for the i^{th} choice" i.e.,

$$\text{decision variable} \quad d_i = max\left(min\left(CCI_i,\ ACI_i\right)\right). \qquad (9)$$

Table 7
After reorientation, the current and the interfering BS for ACI calculations

Wedge	Current BS (after reorientation)	Interfering BS (ACI)		
		dominant	less dominant	
1	(2, 2)	(6, 4)	–	–
2	(0, 2)	(−4, 8)	(−4, 12)	–
3	(2, 0)	(6, −2)	(10, −2)	(10, −6)
4	(2, 2)	(6, 4)	–	–

Table 8
Approximate areas within the cell that experience different levels of ACI before and after reorientation of R_x antennas

C/I value [dB]	Approximate areas [%]	
	before reorientation	after reorientation
Below 10	0.10	0.17
Below 15	0.83	1.18
Below 20	2.71	3.43
Below 25	8.08	9.07
Below 30	14.66	15.55
Above 30	85.33	84.44

3.3. Reorientation under the constraint of system availability

In actual scenarios, reorientation of receiver antennas at all locations is not possible because of the system availability

Table 9
Approximate areas [%] within the cell that experience different levels of interference after the reorientation of R_x antennas, with and without system availability constraint ($p = 0.01\%$ and receiver $HPBW = 2.4^\circ$)

C/I value [dB]	CCI		ACI	
	without constr.	99.7% sys. avail.	without constr.	99.7% sys. avail.
Below 10	0	0.16	0.03	0.00
Below 15	0.51	2.35	0.50	0.42
Below 20	0.52	3.46	1.84	1.57
Below 25	1.54	5.71	5.46	5.06
Below 30	1.58	6.04	10.88	10.18
Above 30	98.42	93.95	89.11	89.81

constraint. If we try to orient the receiver antennas to far off alternate base stations, the LOS may not exist due to tall buildings and foliage. To get a feel for the performance due to the system availability constraint, we put in the following restriction: we do not reorient those receiver antennas for which the alternate base station locations are more than 1.5 times the cell radius (one side of our square cell). This factor, r, equal to 1.5 approximately corresponds to 99.7% system availability. The results of the CCI and ACI with this constraint is given in Table 9 for $p = 0.01\%$.

Table 10
Approximate areas [%] within the cell that experience different levels of interference before reorientation of receiver antennas

R_x *HPBW*	C/I value [dB]	$p = 0.01$		$p = 0.001$	
		CCI	ACI	CCI	ACI
2.4°	Below 10	0.79	0.03	2.60	0.07
	Below 15	6.13	0.40	6.95	0.64
	Below 20	9.89	1.56	11.53	2.15
	Below 25	13.15	4.68	13.57	6.43
	Below 30	14.01	9.80	14.11	11.36
	Above 30	85.98	90.19	85.89	88.64
5.0°	Below 10	1.61	0.05	5.48	0.16
	Below 15	12.30	0.85	15.14	1.38
	Below 20	20.40	3.35	22.24	4.63
	Below 25	25.24	9.84	27.33	13.44
	Below 30	29.34	20.76	29.87	24.58
	Above 30	70.65	79.24	70.12	75.41

Table 11
Approximate areas [%] within the cell that experience different levels of interference after reorientation of R_x antennas

R_x *HPBW*	C/I value [dB]	$p = 0.01$		$p = 0.001$	
		CCI	ACI	CCI	ACI
2.4°	Below 10	0.16	0.00	0.43	0.05
	Below 15	2.35	0.42	2.57	0.74
	Below 20	3.46	1.57	5.02	2.30
	Below 25	5.71	5.06	5.87	7.22
	Below 30	6.04	10.18	6.08	11.73
	Above 30	93.95	89.81	93.92	88.26
5.0°	Below 10	0.23	0	1.42	0.12
	Below 15	5.32	0.72	7.70	1.45
	Below 20	10.60	3.01	12.39	4.50
	Below 25	13.45	9.51	16.34	13.30
	Below 30	17.59	19.58	17.80	22.97
	Above 30	82.40	80.41	82.19	77.02

It can be observed that, under this constraint, there is a decrease in the system performance with respect to the CCI, as expected. However, there is an improvement in the levels of ACI. This is because, in the first case where we reorient with the sole objective to reducing CCI, in many cases we end up increasing the ACI in the process. However, when we reorient under the system availability constraint, we only reorient some of the receiver antennas. In order to get a feel for the typical and the worst case scenarios, we obtain the CCI and ACI for receiver *HPBW* of 2.4° (typical) and 5° (worst case). We also carried out simulations for $p = 0.01$ (typical) and $p = 0.001$ (strict). The interference levels before and after reorientation are tabulated in Table 10 and Table 11 respectively.

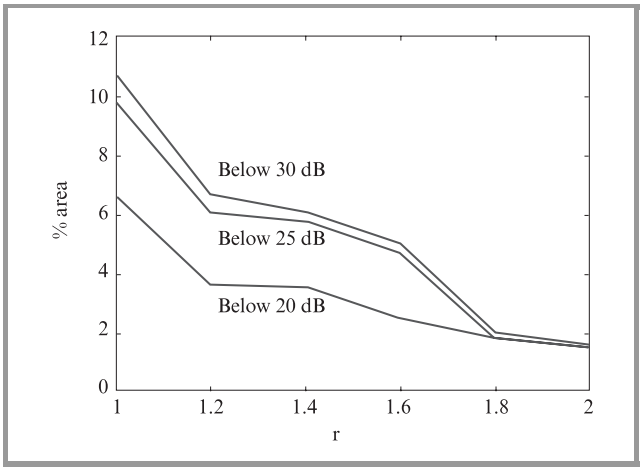

Fig. 10. The percentage of areas in the cell (after reorientation of receiver antennas) versus the multiplicative factor r which determines the system availability.

The extra restriction of the system availability constraint results in a degradation in the system performance, as indicated earlier. In Fig. 10 we plot the percentage of areas in the cell (after reorientation of receiver antennas) versus the multiplicative factor r which determines the system availability. For example, $r = 1.5$ implies that receiver antennas will be reoriented to an alternate BS if the LOS distance does not exceed 1.5 times the cell radius. This corresponds to system availability of 99.7%.

4. Conclusions

In this paper we have investigated the intra-cell interference as well as LOS cochannel and adjacent channel interference for the LMDS architecture. Simulations have beenperformed at 42 GHz. Our reflection measurements and multipath propagation studies have shown, that even for very directional customer antennas ($HPBW = 2°$) strong mulipath components might occur and that they are not neglectable. Therefore, the multipath propagation has to be considered in the design of the equalizer of the receiver.

It has been observed that about $10 \div 15\%$ of the areas suffer from interference problems (for an acceptable threshold

of $C/I > 20$ dB) under LOS and clear weather conditions when cell dimensions of about 2 km are deployed. An interesting thing that has been observed is that for a fixed percentage p, the percentage of cell area below these C/I threshold levels firstly increases with the cell dimension L, reaching its peak value at about 3 km, and then decreases again. The LOS interference problem will be reduced if the *HPBW* of the subscriber's antennas are decreased down to 2°, which means comparatively large antenna diameters of up to 25 cm and more difficulties of arranging them to point precisely to the base station, thus suffering some alignment losses.

In the latter portion of the paper we have proposed a simple technique to reduce the cochannel interference simply by reorienting the receiver antennas to a more favourable base station. It was observed that by reorientation, the area encountering CCI below 30 dB was decreased from 19.1% to 3.4%. This big improvement comes at no additional cost. The ACI values remain comparable to those prior to reorientation. If the system availability constraint is put, we still observe a big improvement, though not as large as without any constraint. Further improvement is possible if we check every receiver location and see whether the reorientation to reduce CCI or ACI produces a better result.

References

[1] CTS Project 215, "Cellular Radio Access for Broadband Services (CRABS)", Feb. 1999, pp. 18–19.

[2] ITU-R Rec. 452-6, "Prediction Procedure for the Evaluation of Microwave Interferrence between Stations on the surface of the Earth at Frequencies above 0.7 GHz", PN Series, Propagation in Non Ionized Media, 1990, pp. 565–591.

[3] A. Seville, M. Willis, and E. Falaise, "Area coverage studies for millimetre-wave services", in *Millennium Conf. Anten. Propag.*, Davos, Switzerland, Apr. 2000.

[4] R. Jakoby and M. Grigat, "MMDS zur Erweiterung von BK-Netzen", Research Report from the Research Center of Deutsche Telekom AG, 1996.

[5] P. B. Papazian, G. A. Hufford, R. J. Achatz, and R. Hoffman, "Study of the local multipoint distribution service radio channel", *IEEE Trans. Broadcast.*, vol. 43, no. 2, pp. 1–10, 1997.

[6] A. Hayn and R. Jakoby, "Propagation and standardization issues for 42 GHz digital microwave video distribution system (MVDS)", in *Tech. Rep. COST 259 TD (99) 021*, Thessaloniki, Greece, Jan. 1999.

[7] A. Hayn, G. Bauer, J. Freese, and R. Jakoby, "Entwicklung von Ausbreitungsmodellen und Software-modulen zur Abschätzung der MWS-Versorgung unter Berücksichtigung von abgeschatteten Bereichen", Research Report for T-Nova, Deutsche Telekom, Nov. 1999.

[8] W. S. Ament, "Toward a theory of reflection by a rough surface", *Proc. IRE*, vol. 41, no. 1, pp. 142–146, 1953.

[9] L. Boithias, *Radio Wave Propagation*, New York: McGraw-Hill, 1987.

[10] G. Bauer, J. Freese, and R. Jakoby, "Single-cell coverage prediction of LMDS including passive reflectors", in *ICAP 2001*, Manchester, Apr. 2001.

[11] IEEE 802.16.1pc-00/15, "Proposed System Impairment Models", Feb. 2000.

Ranjan Bose received his B.Tech. in electrical engineering from IIT, Kanpur in 1988 and his M.Sc. and Ph.D. in electrical engineering from the University of Pennsylvania, PA in 1993 and 1995, respectively. He worked as a Senior Design Engineer in Alliance Semiconductors Inc., San Jose, CA from 1996 to 1997. Since November 1997 he is working as an Assistant Professor at IIT, Delhi in the Department of Electrical Engineering. His research interests lie in the areas of broadband wireless access and coding theory. He received the URSI Young Scientist award in 1999 and is currently at the Technical University of Darmstadt, Germany on the Humboldt Fellowship.
e-mail: rbose@ee.iitd.ernet.in
Technische Universität Darmstadt
Institut für Hochfrequenztechnik
Fachgebiet Mikrowellentechnik Merckstrasse 25
D-64283 Darmstadt, Germany

Andreas Hayn received the Dipl.-Ing. (M.Sc.) degree from the Technical University of Darmstadt, Germany in 1997. He is currently working towards the Dr.-Ing. (Ph.D.) degree in electrical engineering at the Institute of Microwave Engineering at the Technical University of Darmstadt. His research interests include the electromagnetic and acoustic wave propagation and broadband wireless radio systems.
e-mail: a.hayn@ieee.org
Technische Universität Darmstadt
Institut für Hochfrequenztechnik
Fachgebiet Mikrowellentechnik Merckstrasse 25
D-64283 Darmstadt, Germany

Rolf Jakoby received the Dipl.-Ing. and Dr.-Ing. degrees in electrical engineering from the University of Siegen, Germany, in 1985 and 1990, respectively. In 1991, he joined the Research Center of Deutsche Telekom in Darmstadt, Germany. There, he has first conducted radiowave propagation research in the Ku- and Ka-band within ESA's

OLYMPUS satellite campaign and in the UHF-band for UMTS mobile communications in urban microcells. Then, he lead a project concerning Local Multipoint Distribution Systems (LMDS) at 42 GHz. In April 1997, he got a professorship for Microwave Technology at the Technical University of Darmstadt, where his research is focused on broadband wireless systems and on adaptive antennas at microwaves. He is a member of the IEEE and the German Society for Information Technology ITG. In Feb. 1992, he received a prize and award for his Ph.D. thesis from the CCI Siegen and in Dec. 1997, a prize and award from the ITG for an excellent scientific publication in the IEEE AP-44, 1996.

e-mail: jakoby@hrzpub.tu-darmstadt.de
Technische Universität Darmstadt
Institut für Hochfrequenztechnik
Fachgebiet Mikrowellentechnik Merckstrasse 25
D-64283 Darmstadt, Germany